SLAC-PUB-1620
January 1976
(T/E)

A PHENOMENOLOGICAL ANALYSIS OF HIGH p_T SPECTRA AND ANGULAR MULTIPLICITY CORRELATIONS IN pp COLLISIONS*

Risto O. Raitio† and Gordon A. Ringland††
Stanford Linear Accelerator Center
Stanford University, Stanford, California 94305

(Contributed paper for Lepton-Photon Symposium,
Stanford University, 21-27 August 1975;
also submitted to Phys. Rev. D.)

*Work supported by the U. S. Energy Research and Development Administration.
†On leave from: University of Helsinki, Helsinki, Finland.
††Present address: Rutherford Laboratory, Chilton, Didcot, Oxfordshire, 0X11 OQX, England.

ABSTRACT

We analyze the high energy and high p_T proton-proton 90^o inclusive spectra in the framework of the constituent interchange model. We perform both single and few term fits to find out whether a small number of hard collision subprocesses can describe the data. We also consider constraints to the fits due to particle ratios. We conclude that the single particle spectra together with particle ratios can be understood within factors of two in the model with a few hard subprocesses and with simple structure functions. Using the above results the quantum number content of particles balancing the high p_T trigger is predicted in the different cases. Next we analyze the data on proton-proton angular multiplicity correlations. We first discuss measurements on the opposite side multiplicity distributions as a function of angle or rapidity. Using a simplifying assumption we calculate these angular multiplicity distributions in the various cases using the dominant subprocesses found in the above described single particle fits. Good qualitative agreement is found with mildly peripheral amplitudes except for the pion triggers.

I. INTRODUCTION

In this paper we report an analysis of certain high p_T phenomena in proton-proton collisions in the framework of the constituent interchange model[1] (CIM). We have analyzed all published 90^o single particle high p_T hadron spectra from the ISR[2,3] and FNAL.[4] Also we have considered the angular distribution of the recoil multiplicity as giving information on the constituent recoil direction and analyzed this within the context of the CIM.

In Section II we briefly summarize the ground rules of phenomenology with the CIM and illustrate these by some specific examples. For different subprocesses the CIM suggests specific forms for the single particle distributions, with, in general, distinct kinematic dependences. Our analysis seeks to determine if a small number of subprocesses dominate, and, if so, to identify them.

In Section III we fit the single particle data in different kinematic regions with a single general CIM term and so determine the powers of p_T^{-2} and ϵ = (missing mass)^2/s appropriate to describe different subsets of the data. From this analysis we identify a number of important constituent subprocesses— though no single subprocess dominates over the presently investigated kinematic region at FNAL and the ISR.

We then took the three dominant terms for each trigger particle and attempted a global fit over the whole kinematic range. We also consider constraints due to particle ratios. The results presented in Section IV show the model with the simplest form for the structure functions gives a good qualitative representation of the data analyzed though, with the constraints imposed, a good quantitative fit was not, in general, achieved. With an eye to analyzing the multiplicity correlation data from the ISR and predicting quantum number correlations, a three-term analysis was made on just the ISR single particle distributions.

In Section V, on the basis of the preceding analyses we predict the quantum number content of the hadrons balancing the large p_T trigger. We emphasize that the measurement of these quantum numbers is a crucial test of general constituent models.

The ISR data on the angular multiplicity of secondaries in the opposite hemisphere[8, 9, 10] to the high p_T trigger at different c.m. angles are discussed and summarized in Section VI. We assume that the trigger particle gives the direction of one outgoing constituent, and that the maximum of the recoil multiplicity angular distribution gives the average direction of the other recoiling constituent. The expectations of various constituent subprocesses for the angular distributions are investigated, in particular the relative importance of the forms of the structure functions and constituent scattering cross sections are analyzed.

Section VII gives the results of our angular correlation fits for $K^{\pm}$, p, $\bar{p}$ triggers, using the dominant subprocesses established in Section IV. Agreement with the data is generally satisfactory.

The recoil distribution against a π trigger was found more difficult to understand and is treated separately in Section VIII. We present a possible solution; however our solution implies a rather special form for the structure function $F_{\pi/p}$.

Our conclusions are given in Section IX.

II. BASIC RULES OF CIM PHENOMENOLOGY

In parton models it is assumed that an incoming hadron A emits a constituent a with a probability $G_{a/A}(x_1)$, where x_1 is the fraction of A's momentum carried by constituent a. The constituent a then interacts with another emitted constituent b producing a final state, c and d, with cross section $d\sigma/dt'$. The constituent c finally produces the trigger particle C with probability $G_{C/c}(x_3)$ together with some other decay products (Fig. 1). This gives rise to a cross section[1]

$$E\,\frac{d\sigma}{d^3p} \simeq \sum_{a,b,c} \int_0^1 dx_1 \int_0^1 dx_2 \int_0^1 dx_3\; F_{a/A}(x_1)\, F_{b/B}(x_2)\, \tilde{F}_{C/c}(x_3)$$

$$\left. /\left(x_1 x_2 x_3^3\right) \times \delta(s'+t'+u')\, \frac{s'}{\pi}\, d\sigma/dt'(s',t') \right|_{\substack{s'=x_1x_2s \\ t'=x_1t/x_3 \\ u'=x_2u/x_3}} \qquad (1)$$

where the structure functions $F_{a/A}(x)$ are related to the probabilities $G_{a/A}(x)$ by $F(x) = xG(x)$ and s', t' and u' are the subprocess invariants.

An important ingredient in the CIM model is that the constituents a, b, c and d are specified in terms of the minimum number of quarks required to carry the constituent quantum numbers. No constraints are placed on the constituent quantum numbers. The CIM has been reviewed in great detail in Refs. 1 and 5. Here we only mention that the inclusive 90° cross section can be written in the limit $\epsilon \to 0$ in the form

$$E\,\frac{d\sigma}{d^3p} = \sum_{i=1}^{N} C_i \left(p_T^2 + m_i^2\right)^{-N_i} \epsilon^{F_i} \qquad (2)$$

where $\epsilon = 1-x_T = 1-2p_T/\sqrt{s}$, m_i^2 is a free parameter, N_i = (number of active quarks in the subprocess) -2, and $F_i = 2\times$(number of passive quarks) - 1.

We wish to emphasize that Eq. (2) has been derived only in the limit $\epsilon \to 0$ or $x_T \to 1$. When ϵ is close to unity, that is, where most of the measurements have been done, Eq. (2) is multiplied by a smooth function of ϵ. This function decreases quite rapidly as $\epsilon \to 1$ therefore changing the effective power of ϵ. Another fact worth noticing is that the structure functions F(x) in Eq. (1) are not accurately known in the small x ($\epsilon \approx 1$) region. The power behavior $(1-x)^N$ using the counting rules is derived for large x only. At small x, $\nu W_2(x)$ or $F_2(x)$ is known to level off or perhaps decrease towards $x \to 0$ as we shall also find later in the angular correlation analysis. This small x behavior of the F's tends also to decrease the effective power of ϵ. On the other hand, the power of ϵ can be easily increased without changing the power of p_T by emitting extra spectator particles, e.g., $c \to C + \pi$.[15] Therefore we have decided to reduce the amount of numerical work with inaccurately known functions and simply accept as a working hypothesis Eq. (2) with the dimensional counting rules.

To familiarize the reader with these counting rules we consider as an example the production of kaons in proton-proton collisions. Out of the many possible subprocesses $a + b \to c + d$ we consider here the $q(qq) \to KB$ contribution only (see Fig. 1). For both K^+ and K^- we count eight quarks in the subprocess giving N=6. The number of spectators is three for the K^+ since $(qq)q \to (q\bar{s})(sqq)$ (q(s) is a nonstrange (strange) quark) is the simplest subprocess. The particle d has in this case strangeness and baryon number. For the K^- instead we need five spectators to obtain the subprocess $(qs)q \to (s\bar{q})(qqq)$; note that (qqq) is this time a nonstrange baryon. Thus the counting rules give

$$E \frac{d\sigma(K^+)}{d^3p} = C \left(p_T^2 + m^2\right)^{-6} \epsilon^5$$

$$E \frac{d\sigma(K^-)}{d^3p} = C' \left(p_T^2 + m'^2\right)^{-6} \epsilon^9$$

A similar remark applies also to the structure function $F_{K/p}(x)$ occurring in later calculations. The counting rules give $F_{a/A}(x) = (1-x)^{2n(\bar{a}A)-1}$, $x \to 1$, where $n(\bar{a}A)$ is the number of quarks in the state $\bar{a}A$. Hence $F_{K^+/p}(x) = (1-x)^5$ but $F_{K^-/p}(x) = (1-x)^9$ in the $x \to 1$ limit.

III. SINGLE TERM FITS TO $pp \to h+X$ ($p_T > 1.5$ GeV/c)

In an attempt to isolate the dominant subprocesses we have fit the 90^o high p_T single particle distributions by the form

$$E \frac{d\sigma}{d^3p} = C \frac{\epsilon^{F_{eff}}}{\left(p_T^2 + m^2\right)^{N_{eff}}} \tag{3}$$

It was immediately apparent that a single term could not give a reasonable representation of the data at both ISR and FNAL energies (see also Refs. 3 and 4). We therefore fitted the data separately in different kinematic regions in order to identify the dominant mechanisms in these different domains. Having isolated two or three subprocesses these were later combined (see Section IV) in an attempt to produce a global fit to both the ISR and FNAL data.

A cursory glance at Table I reveals that a single term fit gives an adequate representation of the $K^\pm$ and $\bar{p}$ spectra, though the powers of p_T^{-2} and ϵ vary as we go from the B-S kinematic region[3] to the C-P region.[4] Specifically for high p_T $K^\pm$ and $\bar{p}$ the power of ϵ decreases and the power of p_T^{-2} increases as we move from the B-S to the C-P kinematic region.

For high p_T π's, we note that a single term is only adequate to represent the CCR or the CCRs data,[2] where the $q\bar{q} \to M\bar{M}$ subprocess appears to be favored. The B-S data is badly fitted, but the subprocess $qM \to qM$ is favored. It was found impossible to obtain any reasonable single term fit to the C-P π data. As shown in Table I separate fits were made to adjacent pairs of the low and high energy data. These fits were very poor, but suggested $q\bar{q} \to M\bar{M}$ as the mechanism for the higher energy pair of distributions, whereas $qM \to qM$ is favored for the lower energy pair.

For p's, a good fit was found for the B-S data, however, in the light of particle ratios it is doubtful whether we can take literally the subprocess indiated; this will be discussed in the next section. No reasonable fit was obtained for the C-P data.

IV. THREE TERM FITS TO $pp \to h + X$ ($p_T > 1.5$ GeV/c)

We first consider the meson single particle spectra from both FNAL and the ISR. Single term fits discussed in the previous section suggested three important subprocesses: $q\bar{q} \to M\bar{M}$, $qM \to qM$ and $qd \to MB$. (We shall henceforth label the diquark system (qq) by d.) We therefore attempted a three term fit of the meson spectra by

$$E \frac{d\sigma}{d^3p} = \sum_{i=1}^{3} C_i \left(p_T + m_i^2\right)^{-N_i} \epsilon^{F_i} \tag{4}$$

where the three terms correspond to the above subprocesses (see Fig. 1). The results of this global fit are presented in Table II.

We first discuss the statistical adequacy of the fits. Even with three or four terms the fits cannot be regarded as quantitatively good. This is compounded by the fact that we used the uncertainty of relative normalizations between experiments to produce the best fit possible. (See footnote to Table II.) We get typically $\chi^2/N_{DF} \sim 10$. Thus the χ^2 is not a very useful measure of the fits considered here. Consequently we calculated the ratio of the CIM cross section to the experimental cross section and found that in the case of protons, which have the largest χ^2/N_{DF}, the model fitted the data within a factor of two.

On the other hand, the C-P data[4] were obtained on a nuclear target (tungsten) and in principle there exists uncertainties as to the reliability of the nuclear corrections which were measured only at $\sqrt{s} = 23.8$ GeV. Comparison with the true pp B-S data at $\sqrt{s} = 23.4$ GeV show the corrections appear to be reliable for $p_T < 2.35$ GeV/c. However as yet no independent checks are available for higher p_T, or for $\sqrt{s} = 19.4$ and 27.4 GeV.

We next discuss the relative strength of the subprocesses. For π production over the ISR-FNAL region so far explored we see that the two subprocesses $q\bar{q} \rightarrow M\bar{M}$ and $qd \rightarrow MB$ are dominant, with the former reaction more important. This may lead to a difficulty for some constituent models. Combridge[6] has shown that if $q\bar{q} \rightarrow M\bar{M}$ is the dominant process in giving rise to high p_T pions in proton-proton collisions, then since a $\bar{q}$ is far easier to find in a meson, the invariant cross sections for high p_T pions in pion-nucleon collisions should be 2-3 orders of magnitude higher. However, another calculation has been made by Blankenbecler[16] using $q\bar{q} \rightarrow M\bar{M}$, $qM \rightarrow qM$ and $qd \rightarrow MB$ terms both for π^- and p induced π^0 spectra yielding only 1-10 times more π^0's with the π^- beam for $x_T < 1/2$. Data in this region on $\pi^- p \rightarrow \pi^0 + X$ from FNAL[7] indicate that the ratio of this cross section to the $pp \rightarrow \pi^0 + X$ cross section is close to unity.

For K^+ and K^- the dominant subprocess is $qd \rightarrow MB$. The $q\bar{q} \rightarrow M\bar{M}$ and $qM \rightarrow qM$ process are very small contrary to expectations from our π fits and symmetry arguments. Note that the K^- spectrum requires an ϵ^9 term in contrast to the ϵ^5 term for K^+. This difference is just what is expected on the basis of the two additional spectator quarks needed in K^- production.

We now consider the p and $\bar{p}$ spectra. We first made independent fits to both p and $\bar{p}$ distribution using $qd \rightarrow MB$, $q\bar{q} \rightarrow B\bar{B}$ and $BB \rightarrow BB$ terms (see Fig. 1b) for the protons and $q\bar{q} \rightarrow B\bar{B}$ and $M\bar{M} \rightarrow B\bar{B}$ for the antiprotons. The χ^2/N_{DF} we obtained were 75/42 for the protons and 456/42 for the antiprotons. Although the proton fit is excellent statistically it was suspect for the following reasons: (i) the mass squared parameters in Eq. (4) were all very large:

3.5 - 8.6 GeV^2, (ii) the fit implies p/π^{+-o}, p/K^+ and $p/\bar{p}$ ratios that differ from the experimental values by an order of magnitude or more.

To overcome these difficulties we now constrain the parameters in the fits so that a given subprocess has equal amplitude in all reactions. The simplest choice to perform a constrained fit is to make a joint fit to the proton and antiproton spectra with

$$E\,\frac{d\sigma(p)}{d^3p} = C_1\left(p_T^2+m_1^2\right)^{-10}\epsilon^3(1-\epsilon)^2 + C_2\left(p_T^2+m_2^2\right)^{-6}\epsilon^5 + C_3\left(p_T^2+m_3^2\right)^{-6}\epsilon^{11} + C_4\left(p_T^2+m_4^2\right)^{-8}\epsilon^{11} \tag{4a}$$

$$E\,\frac{d\sigma(\bar{p})}{d^3p} = C_3\left(p_T^2+m_3^2\right)^{-6}\epsilon^{11} + C_4\left(p_T^2+m_4^2\right)^{-8}\epsilon^{11} \tag{4b}$$

and $m_i^2 \leq 3$ GeV^2, i=1, . . . , 4. These contributions are justified partly by the results of the single term fits and partly by "trial and error" search method. The results of this joint fit are indicated in Table II. We see that the proton fit now is much worse statistically and the antiproton fit has somewhat larger χ^2. On the other hand, the proton meson ratios, as implied by the qd → MB process, are now substantially closer to the data. At the ISR reference point $\sqrt{s}$ = 44 GeV, $p_T \simeq 2.5$ GeV/c we have that the ratios $(p/\pi^{+-o})_{CIM}/(p/\pi^{+-o})_{expt}$ and $(p/K^+)_{CIM}/(p/K^+)_{expt}$ all are between .99 and 2.1. In the FNAL measurements at $\sqrt{s}$ = 27 GeV, p_T=6.9 GeV/c the same ratios are all between 2.2 and 2.9. These ratios are, needless to say, as good as one could hope since no constraints were set on the qd → MB term. Thus it seems that in the unconstrained p and $\bar{p}$ fits fixing the $q\bar{q} \to B\bar{B}$ contribution, which was too large in the p and too small in the $\bar{p}$ case, has stabilized in an interesting way the qd → MB term which gives rise to proton-antiproton and proton-meson ratios close to the data. To illustrate the above points we show the $\bar{p}/p$ ratio from the joint fit in

Fig. 2. As expected from Eqs. (4a) and (4b) it is always below 1 because the large term qd $\rightarrow$ MB contributes only in the proton spectrum. The ratio is off the data by a factor of two roughly. Note that the unconstrained p and $\bar{p}$ fit gives a better $\bar{p}/p$ ratio (see Fig. 2).

Since in Sections VI - VIII, we shall consider angular correlations in the ISR region, we have also made few term fits solely in that kinematic region to check the dominant subprocesses. Here again we first made unconstrained fits to all particle spectra. The meson results are shown in Table III. The proton and antiproton fits were also good with χ^2/N_{DF} = 26/20 and 36/20, respectively. But again the p/π and p/K^+ ratios were off roughly by an order of magnitude. Next we repeated the technique of making a constrained joint fit to the p and $\bar{p}$ spectra using Eqs. (4a) and (4b). The resulting p/π and p/K^+ ratios at the reference point $\sqrt{s}$ = 44 GeV and p_T = 2.5 GeV/c deviate now from the data by factors 1.6 and .5, respectively. The $\bar{p}/p$ ratio has not changed much from the FNAL and ISR fit.

As expected from the single term studies the statistical quality of the ISR fits is clearly better than the FNAL and ISR fits. This, of course, says little about the global applicability of the model but gives us confidence in picking the relevant subprocesses in the ISR region. Note also that the angular dependence of the single particle fits seems to be weak at least in the $30^o - 90^o$ trigger angle region.[3]

Let us finally summarize this long section. For all mesons we found that the important subprocesses are qd $\rightarrow$ MB, $q\bar{q} \rightarrow M\bar{M}$, and qM $\rightarrow$ qM. The $q\bar{q} \rightarrow M\bar{M}$ contribution must be very small, however, in the light of the FNAL $\pi p \rightarrow \pi^o + X$ data. This indicates a problem in determining the power of ϵ using the counting rules. For protons and antiprotons the most important contributions are qd $\rightarrow$ MB and $q\bar{q} \rightarrow B\bar{B}$. Thus we conclude that a few subprocesses of simple type give the bulk of $E\frac{d\sigma}{d^3p}$ for all detected particles. Using these contributions both the single particle spectra and the particle ratios can be fitted approximately within a factor of two.

V. QUANTUM NUMBER CORRELATION PREDICTIONS

A very important property of constituent models is that they predict the overall quantum numbers of the state recoiling against the observed high p_T trigger. Where the recoil state is a quark, we suppose that the seen recoil quantum numbers are π like if the quark is u or d, and K like if the quark is s.

In Table IV we present the predictions of our constituent model analyses for the quantum number correlations associated with a variety of high p_T triggers at ISR energies.

A particularly interesting prediction is the large fraction of events with a $K^{\pm}$ trigger which should have a baryon in the recoil "jet". One should also note the variation of the quantum number content of the recoil as $\sqrt{s}$ and p_T change. This, of course reflects the relative importance of different sub-processes as the kinematic region is varied. We regard such tests as central to the question of the relevance of constituent models to high p_T phenomena, and for further elucidation of the underlying mechanisms.

VI. ANGULAR CORRELATION RESULTS AND A PRIORI EXPECTATIONS FROM CONSTITUENT MODELS OF HIGH p_T PHENOMENA

We have emphasized in Section V the importance of quantum number correlations between the high p_T trigger particle and the hadrons (away-side) balancing the transverse momentum of the trigger particle. Though no such correlation data is presently available, data currently exists on the angular distribution of the particles balancing the high p_T trigger, and of especial interest, data at different trigger particle angles. Associated multiplicity data, all from the ISR include:

1) The Daresbury-Illinois-Liverpool-Rutherford (DILR) results[8] with high p_T trigger of $\pi^{\pm}$, $K^{\pm}$, p, $\bar{p}$; at c.m. angles of 90°, $62\frac{1}{2}^{\circ}$ and 45°, and $\sqrt{s} = 44$ GeV.

2) The Aachen-CERN-Heidelberg-Munich (ACHM) data[9] with a π^{o} trigger at 90° and 55°, and $\sqrt{s} = 52$ GeV.

3) Published data concerning the recoil angular distributions against a π^{o} trigger at 90° and $17\frac{1}{2}^{\circ}$, $\sqrt{s} = 52$ GeV from the Pisa-Stony Brook (P-SB) collaboration.[10]

Two representative samples of the data are shown.

In Fig. 3 we show the polar angular distribution of away-side multiplicity distribution against a π^{+} high p_T trigger at 45° and 90° from the DILR data. The P-SB away-side multiplicities are shown in Fig. 4 for $\gamma(\pi^{o})$ high p_T triggers at 90° and $17\frac{1}{2}$. <u>Our central assumption in interpreting the data is that the maximum of the away-side angular multiplicity distribution gives the average direction of the constituent d recoiling against the constituent c which gives rise to the trigger particle—see Fig. 1a.</u>[20] These multiplicities, for experimental reasons, are normalized. The DILR data are normalized with respect to the multiplicity observed with a low p_T trigger, and in principle this could introduce biases. The P-SB data are normalized with respect to the multiplicity observed with beam-beam triggers, and so there are less likely biases. However the ACHM distributions are absolute and show the same correlations.

The pion trigger data shows that the recoil multiplicity peaks approximately collinearly when the trigger angle is $45^{\circ} \leq \theta_1 \leq 90^{\circ}$. Both the DILR and ACHM data show this effect. However, when the π trigger angle is smaller, say $\theta_1 \sim 20^{\circ}$, the situation seems to be different as seen in Fig. 4. If we take the highest p_T region data at face value the jet is now in the same hemisphere with the trigger; in other words there is evidence for back-antiback structure.

For $K^{\pm}$ and $p, \bar{p}$ triggers at 90°, 62.5° and 45°, the DILR data show that the recoil multiplicity, though a maximum in the plane defined by the trigger and beams, comes off at approximately 90°. These systematics are illustrated in Fig. 5 for $\theta_1 = 45^{\circ}$, and the details are given in Table VI. In short, we analyze the data by assuming that the multiplicity maximum gives the average direction of the recoil "jet".

Having now adopted the view that the peaks in the ISR angular distributions of away-side multiplicity can be understood in terms of constituent scattering producing the trigger and an opposing "jet" we wish to see what kind of results are expected on the basis of general parton model ideas. The two jet (or particle-jet) cross section was derived and its importance emphasized by Bjorken[11] and by Ellis and Kislinger[11] and it is in the c.m. frame (Figs. 1 and 5)

$$\frac{d\sigma}{dp_T^2\, d\theta_1\, d\theta_2} \simeq \sum_{a,b} F_{a/A}(x_1)\, F_{b/B}(x_2)/(\sin\theta_1 \sin\theta_2) \times d\sigma/dt'(s',t')$$

where p_T is the trigger transverse momentum (in the calculations we increase p_T by 50% to account for possible accompanying particles in $c \rightarrow C$) and

$$x_1 = p_T/\sqrt{s}\left(\cot\tfrac{1}{2}\theta_1 + \tan\tfrac{1}{2}\theta_2\right)$$

$$x_2 = p_T/\sqrt{s}\left(\tan\tfrac{1}{2}\theta_1 + \cot\tfrac{1}{2}\theta_2\right)$$

$$s' = (p_a + p_b)^2 = x_1 x_2 s$$

$$t' = (p_a - p_{trigger})^2 = -p_T^2\left(1 + \tan\tfrac{1}{2}\theta_1 \tan\tfrac{1}{2}\theta_2\right)$$

$$d\sigma/dt' \simeq (1/s')^2 \; |A(a+b \to \text{trigger} + \text{jet})|^2$$

The structure function $F_{a/A}(x)$ we assume to have the counting rule form[1] $F(x) = (1-x)^{2n(\bar{a}A)-1}$, $x \to 1$ where $n(\bar{a}A)$ is the number of constituents in the state $\bar{a}A$. This gives $F_{q/p}(x) = (1-x)^3$ and $F_{\pi/p} = (1-x)^5$ for $x \to 1$. The constituent scattering amplitudes are the least known element in our discussion. In fact the basic motivation for two jet phenomenology is extracting the F's and $d\sigma/dt'$, or the invariant amplitude $A(s', t')$, from the data as emphasized in Ref. 11. We shall assume for $A(s', t')$ simple scale invariant forms to compare with the data; a quark pole in s'-channel we parametrize simply as $A \simeq 1/s'$ and a diquark exchange amplitude as $1/t' \; 1/(at'+bu')$.

To develop some feeling for the relative importance of the structure functions and $d\sigma/dt'$ we consider first simple "phase space" examples for mesons, where we take $A(s', t') = 1$. When the trigger is at $\theta_1 = 90^{\circ}$ the jet is, of course, symmetric around $\theta_2 = 90^{\circ}$. A more interesting case is at, say, $\theta_1 = 45^{\circ}$. Here we consider the processes $qq \to Md$, $q\bar{q} \to M\bar{M}$ and $qM \to qM$ with constant matrix element. Because θ_1 and p_T are fixed, changing θ_2 changes also the energy $\sqrt{s'}$ of the hard subprocess. Since now $d\sigma/dt' \simeq (1/s')^2$ the jet prefers to go into the direction where s' is minimized, i.e., back-antiback structure is expected on the basis of phase space alone as seen in Table V for $qM \to qM$. In fact all the above three processes give the peak in θ_2 in the same position within 5°, in clear disagreement with the data. Similarly, the process $qd \to MB$ gives with $A(s', t') = 1$ the maximum in θ_2 at 140°.

We may now use experimental information on $\nu W_2(x)$ to represent $F_{q/p}(x)$ more realistically near $x \sim 0$. It is known from deep inelastic ep data[12] that $F_{q/p}(x)$ has, roughly speaking, a plateau at $0 < x < 0.2$. Therefore it is of interest to investigate the effect on angular distributions if we plateau all F(x)'s at $0 < x < .2$. A calculation shows that in the three cases mentioned above the peak positions are shifted down by $10^{\circ} - 15^{\circ}$, improving agreement with the data. From now on we assume that all F(x)'s have this plateau (see Fig. 6a), except for $F_{\pi/p}(x)$ (see Fig. 6b). Note that this plateauing of the F(x)'s makes $\langle x \rangle$ of the slower constituent a or b larger. This makes the boost parameter v/c between the constituent c.m. scattering frame and the proton-proton c.m. frame smaller and so gives a more back-to-back situation. We also considered the effect of a t'-dependent amplitude, like $(1/t')^n$ on the calculated recoil angle. We find that strong t'-dependence favoring small $|t'|$ pushes the θ_2 distribution towards $\theta_2 \sim 0^{\circ}$. Furthermore, strong peripherality introduces broad double hump structure in $d\sigma/d\theta_2$ at $\theta_1 = 90^{\circ}$, which is inconsistent with the data.

Hence plateaued F(x)'s and mild peripherality are expected to yield an opposing jet at $\theta_2 \sim 90^{\circ}$ with the trigger being at $\theta_1 \sim 45^{\circ}$. This is exactly what happens with simple pole amplitudes, $A \simeq 1/s'$, $1/t'$, $1/u'$ (see Fig. 7) added incoherently, in $qM \to qM$ and $q\bar{q} \to M\bar{M}$ scattering while the $qq \to Md$ gives a peak at $\theta_2 = 100^{\circ}$.

VII. FITS TO THE $K^{\pm}$, p, $\bar{p}$ TRIGGER DATA ON THE AWAY-SIDE ANGULAR MULTIPLICITY CORRELATIONS

From the one term fits to the single particle spectra shown in Table I we see that for $K^{\pm}$ the leading contribution is from $qd \to MB$ diagrams in the DILR data region. This is supported by the three term fits in Table III. The subprocess $qd \to MB$ can have a quark or diquark exchange with the amplitudes $\sqrt{\frac{s'}{t'}}\left(\frac{1}{t'}\right)^2$ and $\frac{1}{t'}\frac{1}{at'+bu'}$, respectively, in a scale invariant theory.[1,17]

For antiprotons both the single and three terms fits indicate one subprocess only: $q\bar{q} \to B\bar{B}$. For protons the situation is more complicated. The single term fit gives $N_{eff}=5.3$, $F_{eff}=3.3$ ($dd \to Bq$ with quark exchange) whereas the three term fit favors a $q\bar{q} \to B\bar{B}$ contribution with a much higher F_{eff}. However the particle ratios lead us to favor the three term fit with $q\bar{q} \to B\bar{B}$.

Calculating $d\sigma/d\theta_1 d\theta_2$ with the various amplitudes mentioned above, we conclude that the quark exchange dipole amplitudes $(1/t')^2$ do not give a good description of any of the data because of too strong peripherality (see Table V). We next try to determine the parameters a and b of the diquark exchange amplitude for the $K^{\pm}$, p and $\bar{p}$ trigger cases. We find that $a/b \sim 5$ works well for K^-, p and $\bar{p}$ whereas $a/b \sim 10$ gives good results for K^+ as seen in Table VI and Fig. 8.

We arrive therefore at a rather simple result for $K^{\pm}$, p and $\bar{p}$. At $\sqrt{s}=44$ GeV, $p_T \sim 3$ GeV/c their production at $90^o \leq \theta_1 \leq 45^o$ implies a jet at $\theta_2 \simeq 90^o$. This can be understood as being due to $qd \to MB$ for $K^{\pm}$ and $q\bar{q} \to B\bar{B}$ for p, $\bar{p}$, both with mildly peripheral exchange amplitudes. It should be noted that the inclusion of the second strongest subprocesses from Table III does not change the results obtained from angular calculations involving only the leading term. (See Table V.)

VIII. FITS TO THE π TRIGGER DATA ON ANGULAR MULTIPLICITY CORRELATIONS

We recall that a π trigger, unlike $K^{\pm}$ and $p^{\pm}$, produces a recoil multiplicity which peaks approximately back-to-back with respect to the trigger at $45^o \leq \theta_1 \leq 90^o$. This is true of the DILR data for $\sqrt{s}=44$ GeV, $\theta_1=62.5$ and 45^o, for π^+ and π^- triggers, also in the ACHM data, $\sqrt{s}=52$ GeV, $\theta_1=55^o$ with a π^o

trigger. There is slightly less clear evidence for back-antiback recoil in the Pisa-Stony Brook data, $\sqrt{s} = 53$ GeV, $\theta_1 = 17\frac{1}{2}^{\circ}$.

Examination of Table V shows that back-to-back configurations do not arise naturally from the set of subprocesses considered. In particular the subprocess indicated as dominant for the π distribution from our data analysis and the quark counting rules, $q\bar{q} \rightarrow M\bar{M}$, gives marked disagreement with the data. For this subprocess the recoil maximum occurs at $\theta_2 \approx 90^{\circ}$, essentially independent of the trigger angle. Further, the properties of this process are highly constrained, since the structure functions are measured in deep inelastic lepton scattering, and, at least within the quark counting rules, there exist no freedom for modification of the constituent cross section.

To investigate what kind of structure functions and constituent cross sections might describe the data we have considered the subprocess $qM \rightarrow qM$. Although this subprocess, giving $E\frac{d\sigma}{d^3p} \propto \frac{\epsilon^9}{\left(p_T^2 + m^2\right)^4}$ is negligible according to our fits, it has the closest form to the subprocess $q\bar{q} \rightarrow M\bar{M}$ which gives $E\frac{d\sigma}{d^3p} \propto \frac{\epsilon^{11}}{\left(p_T^2 + m^2\right)^4}$. Further, as previously remarked, the approximate equality of π and p induced high p_T π-cross sections cast serious doubt on the $q\bar{q} \rightarrow M\bar{M}$ mechanism.[6,7]

For an investigation of the possible mechanism of back-to-back correlations, $qM \rightarrow qM$ has the advantage that the π structure functions are not known experimentally, and also there is some freedom (in the context of CIM) for the form of the constituent cross section ($d\sigma/dt'$). We found the angular distributions were fairly insensitive to $d\sigma/dt'$, in that no forms of $d\sigma/dt'$ consistent with the single particle distributions, could, taken together with structure functions discussed in Section VI and Section VII, give a back-to-back correlation.

This then leaves the freedom to vary $F_{\pi/p}(x)$. We found that a sufficiently severe peaking of $F_{\pi/p}(x)$ around $x \approx .2$ gives a reasonable fit to the 45^o π triggers (see Fig. 8). The form taken (see Fig. 6b) was $F_{\pi/p} = (1-x)^5$, $x > .2$ and $F_{\pi/p} = .15 + .89x$, $x < .2$. Theoretically one would expect $F_{\pi/p} \propto \text{const} + \sqrt{x}$ for small x, since such behavior corresponds to the contribution of Pomeron and the vector and tensor trajectories, respectively. Use of the theoretically more plausible forms for $F_{\pi/p}(x)$ gives the recoil at $\theta_2 \simeq 90^o$. A further problem for the fit using the peaked structure function for $F_{\pi/p}$ is that the recoil direction is essentially determined by the x value of the peak of the structure function, and is largely independent of the trigger particle direction. Therefore though one may represent the 45^o π trigger recoil distribution, the suggested back-antiback structure seen in the P-SB data for $\theta_1 = 17\frac{1}{2}^o$ appears to be a problem for such an approach. Although we are aware that the above difficulties imply that we do not have a completely satisfactory solution, we present the result as a measure of the difficulty of the problem.

IX. CONCLUSIONS

For reasons of definiteness, and geography, our analysis is in the specific framework of the SLAC CIM. However, as remarked by Landshoff,[10] many other models, though using different language, have the same mathematical structure. We therefore hope our conclusions may be of some relevance to constituent models in general.

Summarizing our results:

(i) For the combined FNAL and ISR high p_T data on $pp \to \pi^{\pm}, K^{\pm}, p, \bar{p}$ at 90^o, no statistically satisfactory fit was found with the simple structure functions. The χ^2-best fits lead to unsatisfactory particle ratios. After performing a joint fit to the p and $\bar{p}$ data with proper constraints considerable improvement was found in p/π and p/K^+ ratios. Both the single particle spectra and the above particle ratios were good within a factor of about two. A similar factor of two has been obtained in the parton tests of certain features in the final states of hadron-hadron, lepton-hadron and $e^+e^- \rightarrow$ hadrons collisions.[14]

(ii) The ISR $pp \rightarrow \pi^{\pm o}$, $K^{\pm}$, p, $\bar{p}$ at 90^o data which have a relatively restricted range of p_T, can be reasonably well fitted by the CIM. The fit is not qualitatively different from the FNAL fit. Constraints due to particle ratios were considered as in the case of FNAL and ISR combined data. Also the conclusions are quite similar. The dominant subprocesses in the fit are $qM \rightarrow qM$, $q\bar{q} \rightarrow M\bar{M}$, $q\bar{q} \rightarrow B\bar{B}$, $qd \rightarrow MB$, in the various cases. The markedly different ϵ behavior of K^+ and K^- inclusive cross sections is accounted for by the quark counting rules. These rules also give in our fit an explanation why the $\bar{p}/p$ ratio is near unity in a particular kinematic region and decreases with increasing p_T.

(iii) On the basis of these results we predict quantum number correlations, which are a crucial consequence of constituent models. These predictions can be tested in the near future. In particular we predict that a large fraction of events involving a $K^{\pm}$ high p_T trigger should have a baryon in the recoil particles balancing transverse momentum.

(iv) For the angular correlation measurements with $K^{\pm}$, p, $\bar{p}$ triggers, agreement was found with the present data using $qd \rightarrow MB$ and $q\bar{q} \rightarrow B\bar{B}$ diquark exchange amplitudes. The essential features of the model in the angular analysis turned out to be plateaued structure functions and mildly peripheral hard subprocess amplitudes together with the counting rules. The approximate back-to-back structure with large angle $\pi^{\pm o}$ triggers was not equally well explained in the present analysis.

The following price had to be paid to obtain the above results.

(v) The power F of ϵ^F is not easily determined by the counting rules to agree with all the available data. Variations of two units in F had to be accepted in the meson spectra. This is indicated also by the large angle deep inelastic ep scattering results[18] which indicate the behavior $(1-x)^4$ for the nucleon structure functions instead of the predicted third power. These problems can clearly be studied better when data will be available in the $0.5 < x_T \leq 1$ region. Present measurements are unfortunately restricted to low x_T values.

(vi) A number of dominant subprocesses had to be omitted in our analysis; in particular $qq \rightarrow B\bar{q}$ and $qp \rightarrow qp$ are not supported by the present data. Whether these contribute at large s or x_T values remains to be seen.

(vii) A problem known already for some time to the CIM is the same side correlation effects.[19] This is a very interesting challenge for future model building.

Finally, we think that while the details of the CIM, or of any other parton model for that matter, are not in quantitative agreement with the data, the model(s) still may serve as useful phenomenological guide in the search of regularities in the experimental measurements.

ACKNOWLEDGEMENTS

We wish to thank Prof. S. Drell for warm hospitality extended to us at SLAC. We are greatly indebted to J. Alonso, J. Bjorken, R. Blankenbecler, S. Brodsky, S. Ellis, E. Groves, R. Pearson, C. Sachrajda, and D. Sivers for numerous helpful and illuminating discussions. R.O.R. also thanks the Herman Rosenberg Foundation and the State Science Committee (Finland) for financial support.

REFERENCES

1. Some references for the hard-scattering constituent models for inclusive processes are: R. Blankenbecler, S. Brodsky and J. Gunion, Phys. Rev. D 6, 2652 (1972); Phys. Letters 42B, 461 (1973). P. V. Landshoff, and J. C. Polkinghorne, Phys. Rev. D 8, 4157 (1973); Phys. Letters 45B, 361 (1973). R. Blankenbecler, S. Brodsky and J. Gunion, SLAC-PUB-1585 (1975). Power counting rules were developed by: V. Matveev, R. Muradyan and A. Tavkelidze, Lett. Nuovo Cimento 7, 719 (1973); S. Brodsky and G. Farrar, Phys. Rev. Letters 31, 1153 (1973); and R. Blankenbecler and S. Brodsky, Phys. Rev. D 10, 2973 (1974).
2. F. W. Busser et al., CERN-Columbia-Rockefeller collaboration (CCR), Phys. Letters 46B, 471 (1973); and F. W. Busser et al., Phys. Letters 55B, 232 (1975).
3. B. Alper et al., British-Scandinavian collaboration (B-S), Phys. Letters 47B, 275 (1973); and B. Alper et al., Nuclear Phys. B87, 19 (1975); B. Alper et al., CERN preprint, July 1975.
4. J. W. Cronin et al., Chicago-Princeton collaboration (C-P), Phys. Rev. D 11, 3105 (1975).
5. R. Blankenbecler, S. Brodsky and D. Sivers, SLAC-PUB-1595 (1975), to be published in Phys. Reports.

6. B. L. Combridge, Phys. Rev. D 10, 3849 (1974).

7. Kwan Wu Lai, SLAC seminar, June 1975.

8. Daresbury-Illinois-Liverpool-Rutherford collaboration (DILR), private communication from S. Rock and E. Groves.

9. K. Eggert et al., Aachen-CERN-Heidelberg-Munich collaboration (ACHM), Nucl. Phys. B98, 73 (1975).

10. G. Finocchiaro et al., Pisa-Stony Brook collaboration (P-SB), paper 990, Proc. 17th Int. Conf. on High Energy Physics, London, 1974 (Rutherford Laboratory, U.K., 1974). P. V. Landshoff, Rapporteur talk, ibid., p. V-57.

11. J. Bjorken, Phys. Rev. D 8, 4098 (1973);
S. Ellis and M. Kislinger, Phys. Rev. D 9, 2027 (1974).

12. F. Gilman, Rapporteur talk, Proc. 17th Int. Conf. on High Energy Physics, 1974 (Rutherford Laboratory, U.K., 1974); p. IV-149.

13. S. Ellis, ibid., p. V-23.

14. J. Bjorken, Lectures at the 1975 SLAC Summer Institute on Particle Physics.

15. In fact, these extra particles seem to be required by the same side correlation data. See, e.g., P. Darriulat, Rapporteur talk, Int. Conf. on High Energy Physics, Palermo, 1975.

16. R. Blankenbecler, private communication.

17. We are particularly grateful to R. Blankenbecler, S. Brodsky and C. Sachrajda for informative and helpful discussions on this point.

18. W. Atwood, Stanford Thesis, 1975 (unpublished).

19. For a recent review, see P. Darriulat, ibid.

20. A word of caution is needed here. There is no reliable and simple way to estimate how the multiplicity comes around in the final state in the parton models. Therefore enhancements in multiplicity may not necessarily be related to the jet directions.

TABLE I

Single term fits to $pp \to h+x$ at $\theta^* \simeq 90^o$.

$$E\frac{d\sigma}{d^3p} = C\frac{\epsilon^{F_{eff}}}{\left(p_T^2+m^2\right)^{N_{eff}}}$$

Trigger Particle -h and Experimental Group	Kinematic Region*	χ^2/N_{DF}	N_{eff}	F_{eff}	m^2 $(GeV/c)^2$	Implied Dominant Subprocess
π^o CCR	$23.4 \le \sqrt{s} \le 63.0$ $2.59 \le p_T \le 9.01$	137/86	4.2	10.5	.1	$q\bar{q} \to M\bar{M}$
π^+ B-S	$23.4 \le \sqrt{s} \le 63.0$ $1.54 \le p_T \le 4.75$	124/22	3.8	9.0	0	$qM \to qM$
π^+ C-P	$\sqrt{s} = 19.4,\ 23.8$ $1.53 \le p_T \le 7.63$	426/12	4.0	9.1	0	$qM \to qM$
	$\sqrt{s} = 23.8,\ 27.4$ $1.53 \le p_T \le 8.39$	373/14	4.0	10.6	0	$q\bar{q} \to M\bar{M}$
K^+ B-S	$23.4 \le \sqrt{s} \le 63.0$ $1.54 \le p_T \le 4.75$	43/22	4.5	6.7	1.8	Mixture of $q+(qq) \to MB$ and $qM \to qM$
K^+ C-P	$19.4 \le \sqrt{s} < 27.4$ $1.53 \le p_T \le 6.87$	49/19	6.4	6.0	2.7	$q+(qq) \to MB$
K^- B-S	$23.4 \le \sqrt{s} \le 63.0$ $1.54 \le p_T \le 4.75$	42/22	6.0	10.6	4.0	$q+(qq) \to MB$
K^- C-P	$19.4 \le \sqrt{s} \le 27.4$ $1.53 \le p_T \le 6.87$	37/19	6.4	8.1	3.0	$q+(qq) \to MB$
p B-S	$23.4 \le \sqrt{s} \le 63.0$ $1.54 \le p_T \le 4.75$	32/22	5.3	3.3	1.6	$(qq)+(qq) \to B+q$
p C-P	$19.4 \le \sqrt{s} \le 27.4$ $1.53 \le p_T \le 6.87$	200/18	7.4	4.0	3.0	No obvious term
$\bar{p}$ B-S	$23.4 \le \sqrt{s} \le 63.0$ $1.54 \le p_T \le 4.75$	27/22	5.6	13.5	2.0	$q\bar{q} \to B\bar{B}$
$\bar{p}$ C-P	$19.4 \le \sqrt{s} \le 27.4$ $1.53 \le p_T \le 6.87$	24/18	7.7	8.8	4.0	No obvious term

*$\sqrt{s}$ in GeV , p_T in GeV/c

TABLE II

Three term fits to single particle spectra (FNAL + ISR data with $p_T > 1.5$ GeV/c).

Trigger	χ^2/N_{DF}	Subprocess	N	F	$C_i \times 10^{-25}$	m_i^2/GeV^2	Region of Dominance	% Fraction at $\sqrt{s} = 44$ GeV, $p_T \simeq 2.5$
$\pi^+\pi^o$	907/136	$qM \to qM$	4	9	1.3×10^{-10}	1.89	--	10^{-7}
		$q\bar{q} \to M\bar{M}$	4	11	1.76	1.08	$\sqrt{s} > 23.5$	63
		$qd \to MB$	6	5	.069	1.84	$\sqrt{s} < 23.5$	37
π^-	536/45	$qM \to qM$	4	9	1.5×10^{-5}	.83	--	10^{-2}
		$q\bar{q} \to M\bar{M}$	4	11	.049	1.00	$\sqrt{s} > 31$ or $p_T > 2$	57
		$qd \to MB$	6	5	1.54	1.74	$\sqrt{s} < 31$ or $p_T < 2$	43
K^+	656/42	$qM \to qM$	4	9	.0031	.64	--	16
		$q\bar{q} \to M\bar{M}$	4	11	3×10^{-9}	6.4	--	10^{-6}
		$qd \to MB$	6	5	1.27	1.98	$p_T > 1.5$	84
K^-	225/43	$q\bar{q} \to M\bar{M}$	4	11	9.0×10^{-6}	27.9	--	10^{-4}
		$qM \to qM$	4	13	5.6×10^{-6}	1.38	--	10^{-2}
		$qd \to MB$	6	9	3.75	2.75	$p_T > 1.5$	100
p	705/42	$qd \to MB$	6	5	1.5	2.6	$p_T > 2$	47
		$q\bar{q} \to B\bar{B}$	6	11	1.7	3.0	$\sqrt{s} > 30$ and $p_T < 2$	34
		$M\bar{M} \to B\bar{B}$	8	11	5.2	3.0	--	1
		$BB \to BB$	10	$3(x_T^2)$	2.9×10^5	3.0	$\sqrt{s} < 30$ and $p_T < 2$	18
$\bar{p}$	649/44	$q\bar{q} \to B\bar{B}$	6	11	1.7	3.0	$p_T > 1.5$	97.5
		$M\bar{M} \to B\bar{B}$	8	11	5.2	3.0	--	2.5

Note: CP data are multiplied by 1.19 for mesons and .8 for protons.

Table III

Three term fits to the ISR single particle spectra ($p_T > 1.5$ GeV/c).

Trigger	χ^2/N_{DF}	Subprocess	N	F	$C_i \times 10^{-25}$	m_i^2/GeV^2	Region of Dominance	% Fraction at $\sqrt{s} = 44$ GeV, $p_T \simeq 2.5$
π^o	128/91	$qM \to qM$	4	9	3×10^{-8}	2.19	—	10^{-5}
		$q\bar{q} \to M\bar{M}$	4	11	0.062	0.029	$p_T > 1.5$	84
		$qd \to MB$	6	5	0.28	0.11	—	16
K^+	41/20	$qM \to qM$	4	9	0.038	3.04	$p_T > 3$	40
		$q\bar{q} \to M\bar{M}$	4	11	4×10^{-4}	1.3×10^{-4}	—	2
		$qd \to MB$	6	5	2.16	2.78	$p_T < 3$	58
K^-	31/20	$q\bar{q} \to M\bar{M}$	4	11	0.017	1.47	$p_T > 2.5$	44
		$qM \to qM$	4	13	0.007	1.81	—	12
		$qd \to MB$	6	9	23.2	3.07	$p_T < 2.5$	44
p	80/22	$qd \to MB$	6	5	1.6	3.0	$p_T > 5$	35
		$q\bar{q} \to B\bar{B}$	6	11	5.4	3.0	$\sqrt{s} > 23$	58
		$M\bar{M} \to B\bar{B}$	8	11	1.2	1.2	—	1
		$BB \to BB$	10	$3(x_T^2)$	1.2×10^5	3.0	$\sqrt{s} < 23$	6
$\bar{p}$	57/22	$q\bar{q} \to B\bar{B}$	6	11	5.4	3.0	$p_T > 1.5$	98
		$M\bar{M} \to B\bar{B}$	8	11	1.2	1.2	—	2

TABLE IV

Two particle correlation estimates from ISR fit.

Trigger Particle	Opposing Quantum Numbers B	Opposing Quantum Numbers S	% Fraction of Cross Section $\sqrt{s}$ = 44 GeV p_T = 2.3 GeV/c	% Fraction of Cross Section $\sqrt{s}$ = 53 GeV p_T = 4.7 GeV/c	Subprocess
π^o	0	0	85	97	$qM \rightarrow qM$ $q\bar{q} \rightarrow M\bar{M}$
	1	0	15	3	$qd \rightarrow MB$
K^+	0	0, -1	42	82	$qM \rightarrow qM$ $q\bar{q} \rightarrow M\bar{M}$
	1	-1	58	18	$qd \rightarrow MB$
K^-	0	0, +1	56	84	$qM \rightarrow qM$ $q\bar{q} \rightarrow M\bar{M}$
	1	0	44	16	$qd \rightarrow MB$
p	0	0	35	50	$qd \rightarrow MB$
	1	0	6	--	$BB \rightarrow BB$
	-1	0	58	50	$q\bar{q} \rightarrow B\bar{B}$
	-1	0	1	--	$M\bar{M} \rightarrow B\bar{B}$
$\bar{p}$	1	0	98	100	$q\bar{q} \rightarrow B\bar{B}$
	1	0	2	--	$M\bar{M} \rightarrow B\bar{B}$

TABLE V

Expectations for peak positions in jet angular distributions, $\sqrt{s}$ = 44 GeV, p_T(trigger) = 3 GeV/c.

Trigger	θ_1	θ_2^m(CIM)	Subprocess, amplitude
meson	90°	90°	$qM \to qM$
	45°	120°	Phase Space
	$17\frac{1}{2}^\circ$	105°	No plateaus in $F_i(x)$
meson	90°	90°	$qM \to qM$ [a]
	45°	120°	$1/s' + 1/t'$
	$17\frac{1}{2}^\circ$	105°	No plateaus in $F_i(x)$
meson	90°	90°	$q\bar{q} \to M\bar{M}$
	45°	80°	$1/t'$
	$17\frac{1}{2}^\circ$	90°	
meson	90°	$25^\circ + 155^\circ$	$qd \to MB$
	45°	25°	$(1/t')^2$
	$17\frac{1}{2}^\circ$	25°	
baryon	90°	$35^\circ + 145^\circ$	$qp \to qp$
	45°	160°	$1/t'\ 1/(t' + .2u')$
	$17\frac{1}{2}^\circ$	160°	
baryon	90°	$25^\circ + 155^\circ$	$dd \to Bq$
	45°	25°	$(1/t')^2$
	$17\frac{1}{2}^\circ$	25°	
baryon	90°	$35^\circ + 145^\circ$	$qd \to MB$
	45°	55°	$(1/t')^2$
	$17\frac{1}{2}^\circ$	55°	

[a] This case has also been considered by S. Ellis,[13] who finds similar results.

TABLE VI

Fits to the peak positions in jet angular distributions,
$\sqrt{s}$ = 44 GeV, p_T(trigger) = 3 GeV/c.

Trigger	θ_1	θ_2^m(expt)	θ_2^m(CIM)	Subprocess
$\pi^{\pm}$ [8]	90^o	90^o	90^o	$qM \to qM$
	45^o	65^o	65^o	
$\pi^o(\sqrt{s}=53)$ [9]	55^o	55^o	70^o	
$\gamma(\pi^o)(\sqrt{s}=53)$ [10]	$17\frac{1}{2}^o$	120^o [a]	60^o	
K^+ [8]	90^o	90^o	90^o	$qd \to K^+B$
	45^o	90^o	100^o	a/b = 10
	$17\frac{1}{2}^o$	-	125^o	
K^- [8]	90^o	90^o	90^o	$qd \to K^-B$
	45^o	90^o	80^o	a/b = 5
	$17\frac{1}{2}^o$	-	90^o	
p [8]	90^o	90^o	90^o	$q\bar{q} \to p\bar{B}$
	45^o	90^o	85^o	a/b = 5
	$17\frac{1}{2}^o$	-	105^o	
$\bar{p}$ [8]	90^o	90^o	90^o	$\bar{q}q \to \bar{p}B$
	45^o	80^o	75^o	a/b = 5
	$17\frac{1}{2}^o$	-	125^o	

[a] The lower p_T range ($p_T \leq 2.0$) of the $17\frac{1}{2}^o$ P-SB data[10] clearly indicate a back-antiback configuration. This is the p_T region where the DILR data are weighted. However the highest p_T bin, $2.5 < p_T < 3.0$ has a rather broad peaking, $90^o < \theta_2 < 160^o$.

FIGURE CAPTIONS

1. (a) General constituent hard scattering contribution for $A+B \rightarrow C+X$ at high p_T. (b) Specific CIM diagrams for single particle distributions. All lines are quark lines in (b).
2. $\bar{p}/p$ ratio as a function of p_T at $\sqrt{s}=44$ GeV. The dots are the experimental values, the dashed curve is from the unconstrained $\bar{p}$ and p fits and the solid curve is from the constrained joint fit.
3. DILR angular away-side multiplicity data with π^+ trigger at 90° and 45°.
4. P-SB angular away-side multiplicity data with $\gamma(\pi^0)$ trigger at 90° and $17\frac{1}{2}^\circ$ (normalized to multiplicities in beam-beam collisions). Note that in this figure $\theta_2 = \theta - 180^\circ$.
5. Schematic representation of the data on relation of the maximum of the recoil multiplicity with respect to the trigger particle and angle, at $\theta_1 \sim 45^\circ$.
6. (a) The various structure functions used in the calculation of the jet-jet angular distributions. (b) $F_{\pi/p}$ used for our best fit to the recoil against a π trigger.
7. Exchange diagrams used in the angular correlation analysis.
8. Constituent recoil angular distributions against a 45° trigger.

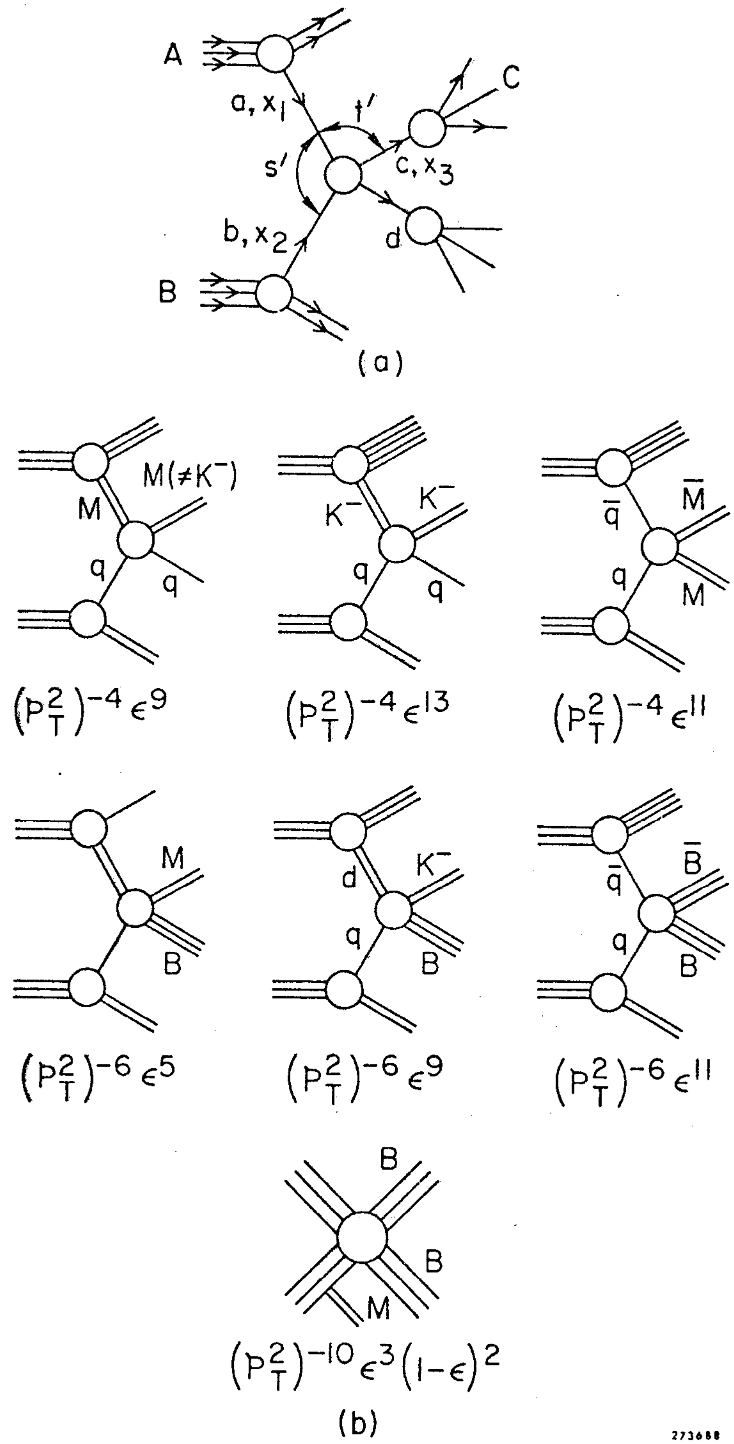
A
B
a, x_1
b, x_2
t'
s'
c, x_3
C
d
(a)
$M(\neq K^-)$
M
q
q
$(P_T^2)^{-4}\epsilon^9$
K^-
K^-
q
q
$(P_T^2)^{-4}\epsilon^{13}$
$\bar{q}$
$\bar{M}$
q
M
$(P_T^2)^{-4}\epsilon^{11}$
M
B
$(P_T^2)^{-6}\epsilon^5$
d
K^-
q
B
$(P_T^2)^{-6}\epsilon^9$
$\bar{q}$
$\bar{B}$
q
B
$(P_T^2)^{-6}\epsilon^{11}$
B
B
M
$(P_T^2)^{-10}\epsilon^3(1-\epsilon)^2$
(b)
273688

Fig. 1

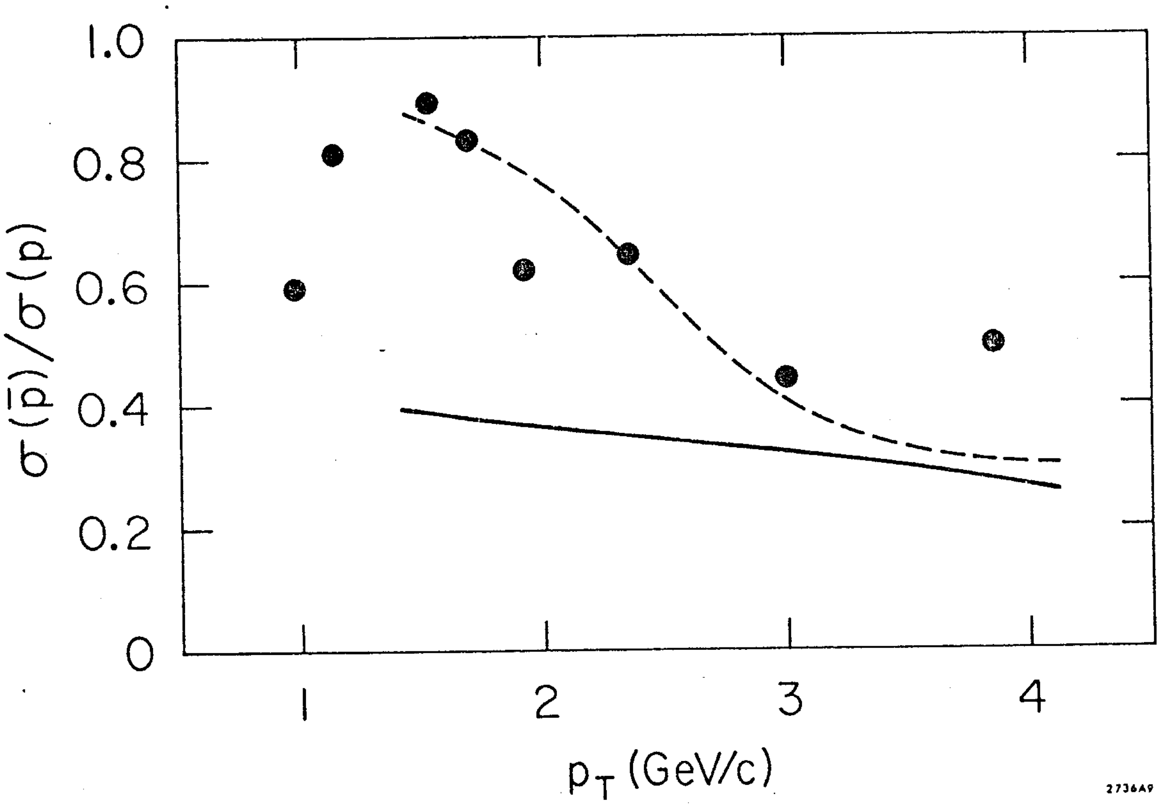

Fig. 2

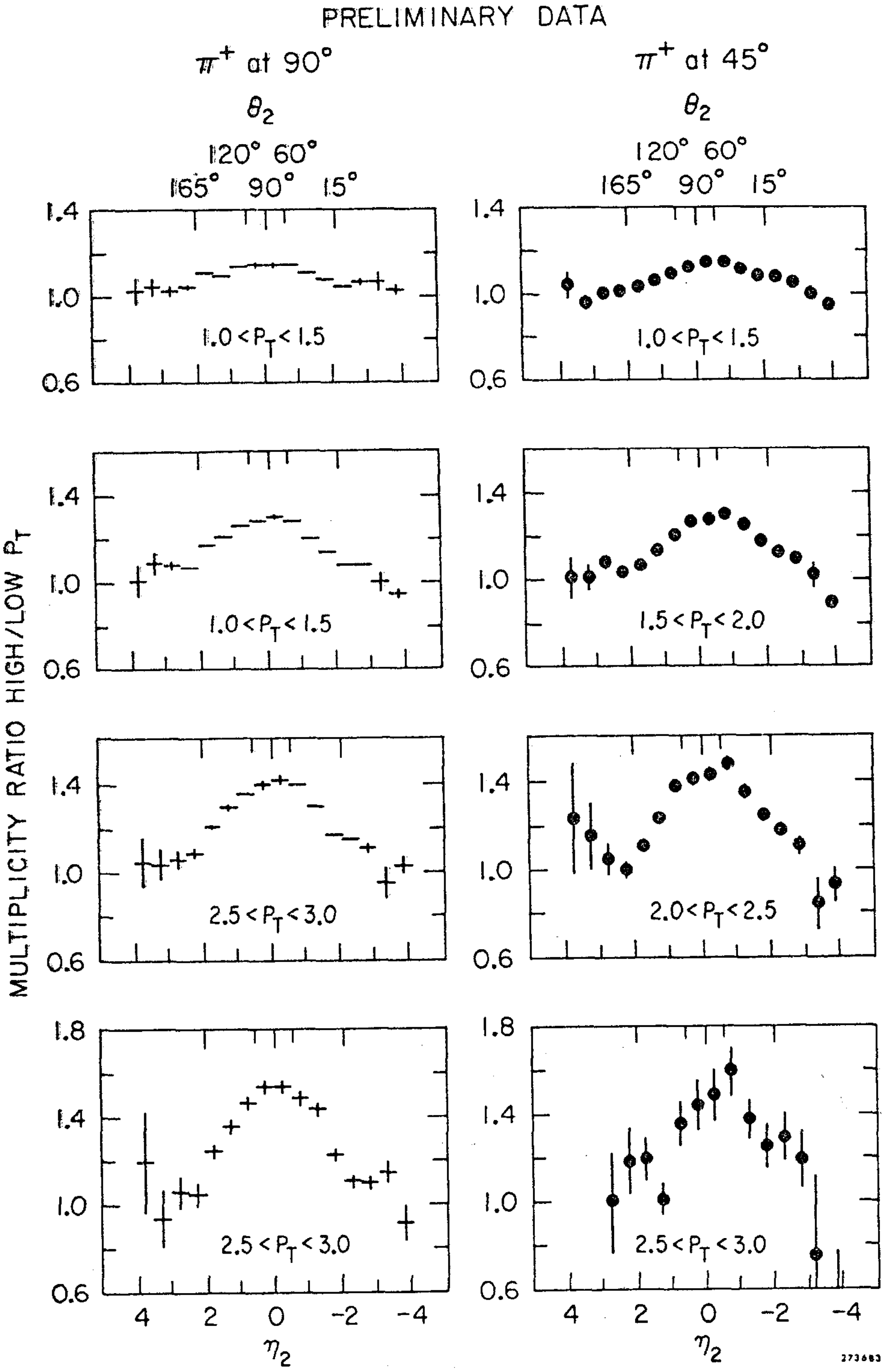
PRELIMINARY DATA
π+ at 90°
π+ at 45°
θ2
120° 60°
165° 90° 15°
MULTIPLICITY RATIO HIGH/LOW PT
1.0 < PT < 1.5
1.5 < PT < 2.0
2.5 < PT < 3.0
2.0 < PT < 2.5
η2
273683

Fig. 3

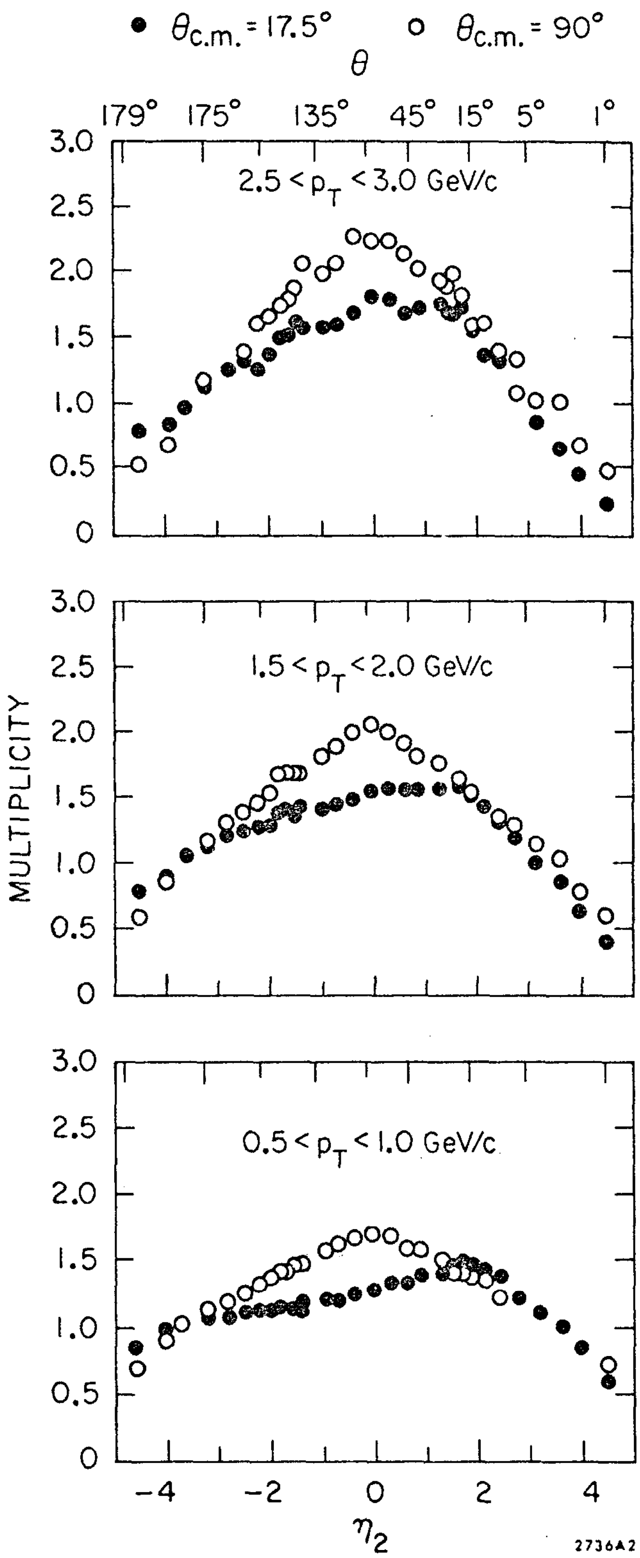

● $\theta_{c.m.}$ = 17.5°
○ $\theta_{c.m.}$ = 90°
θ
179°
175°
135°
45°
15°
5°
1°
2.5 < p_T < 3.0 GeV/c
1.5 < p_T < 2.0 GeV/c
0.5 < p_T < 1.0 GeV/c
MULTIPLICITY
3.0
2.5
2.0
1.5
1.0
0.5
0
−4
−2
0
2
4
η_2
2736A2

Fig. 4

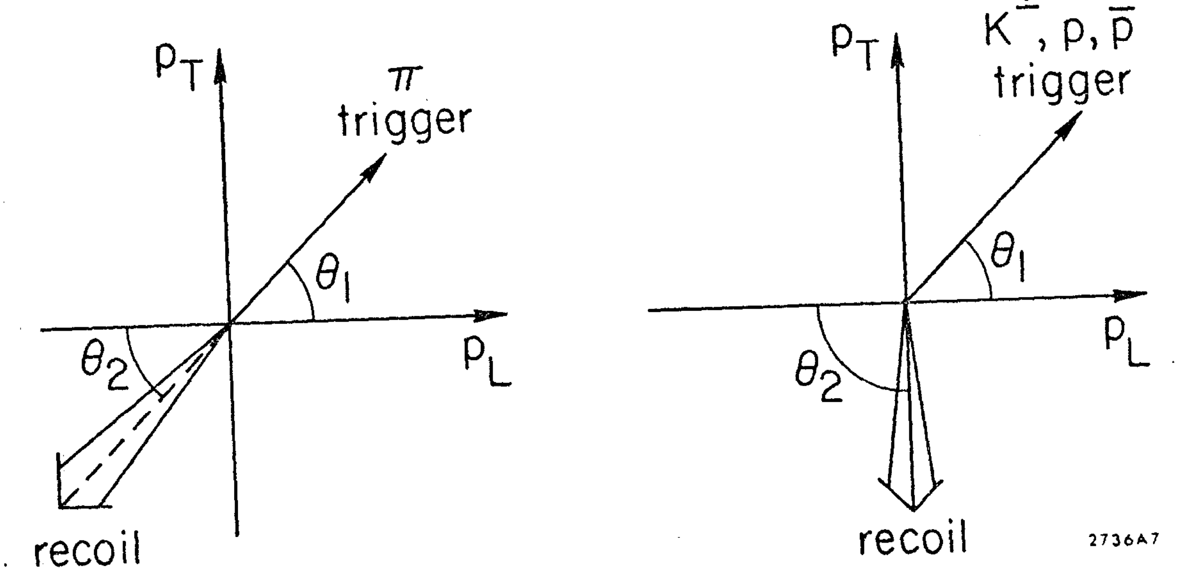

p_T
π
trigger
θ_1
θ_2
p_L
recoil
p_T
$K^{\pm}, p, \bar{p}$
trigger
θ_1
θ_2
p_L
recoil
2736A7

Fig. 5

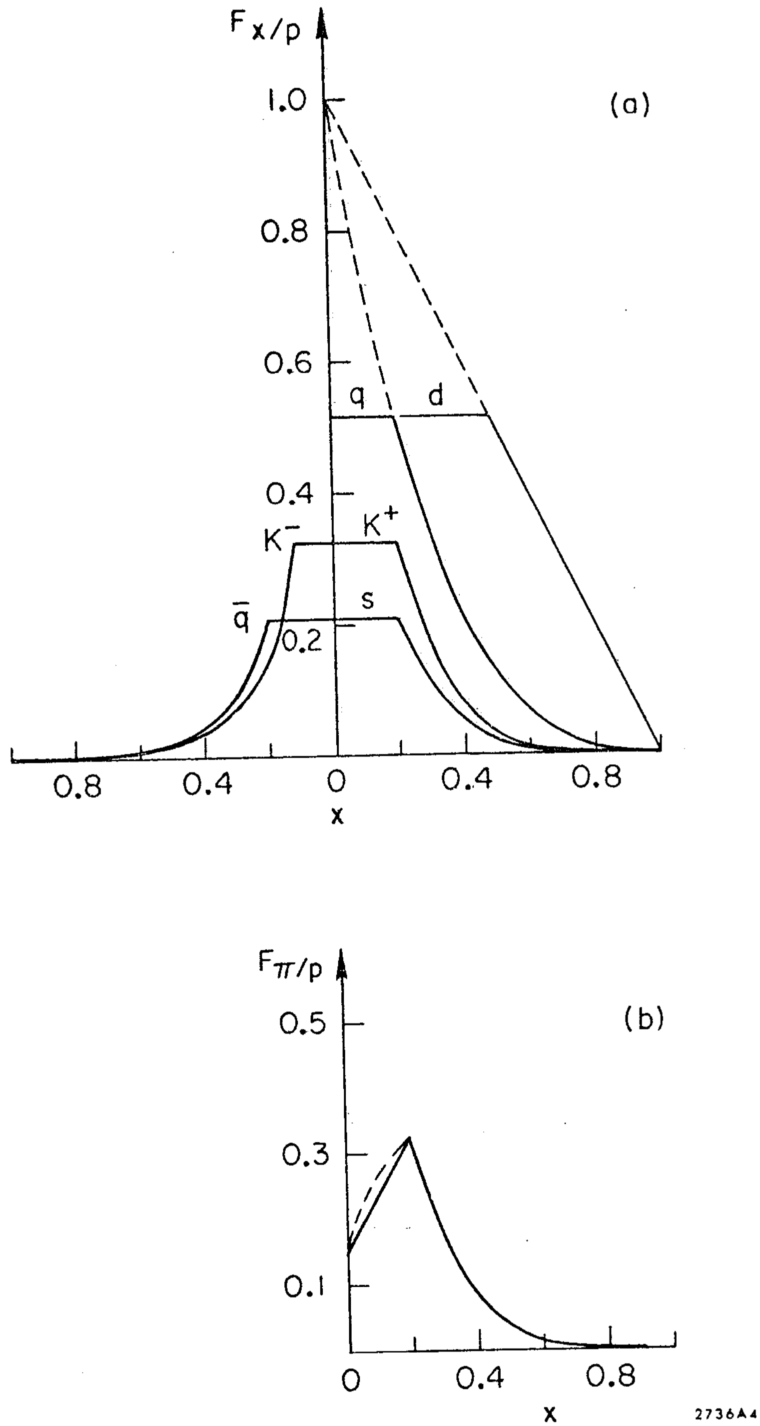

Fx/p
1.0
0.8
0.6
0.4
0.2
(a)
q
d
K⁻
K⁺
q̄
s
0.8
0.4
0
0.4
0.8
x
Fπ/p
0.5
0.3
0.1
(b)
0
0.4
0.8
x
2736A4

Fig. 6

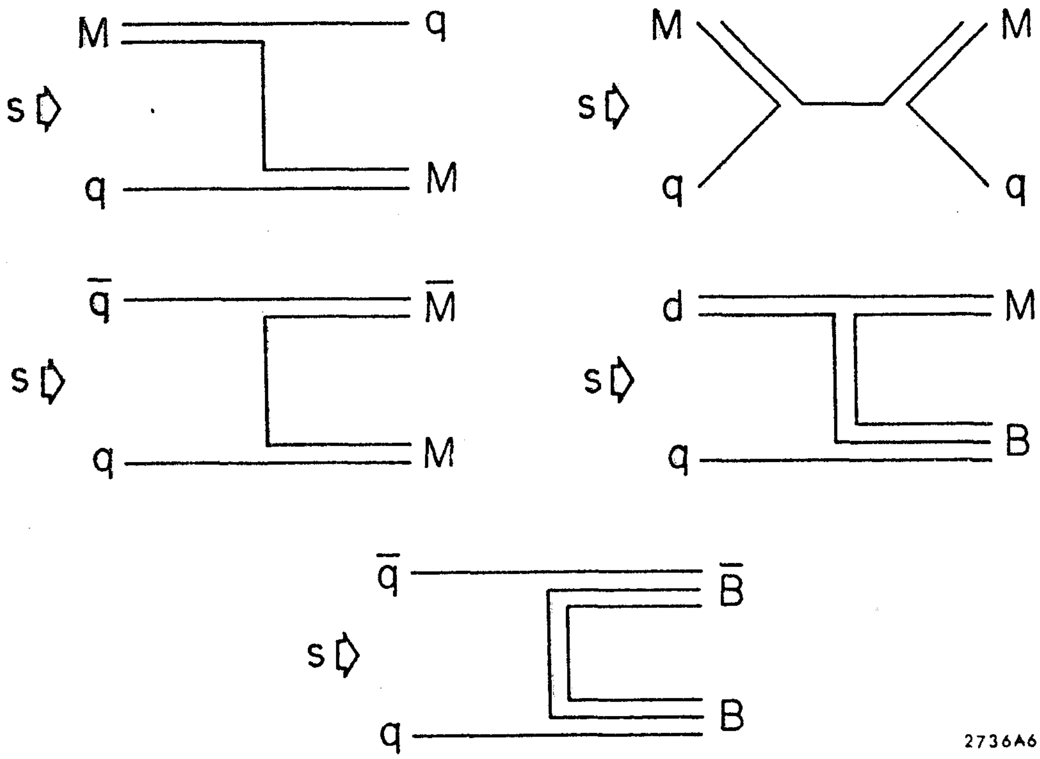

Fig. 7

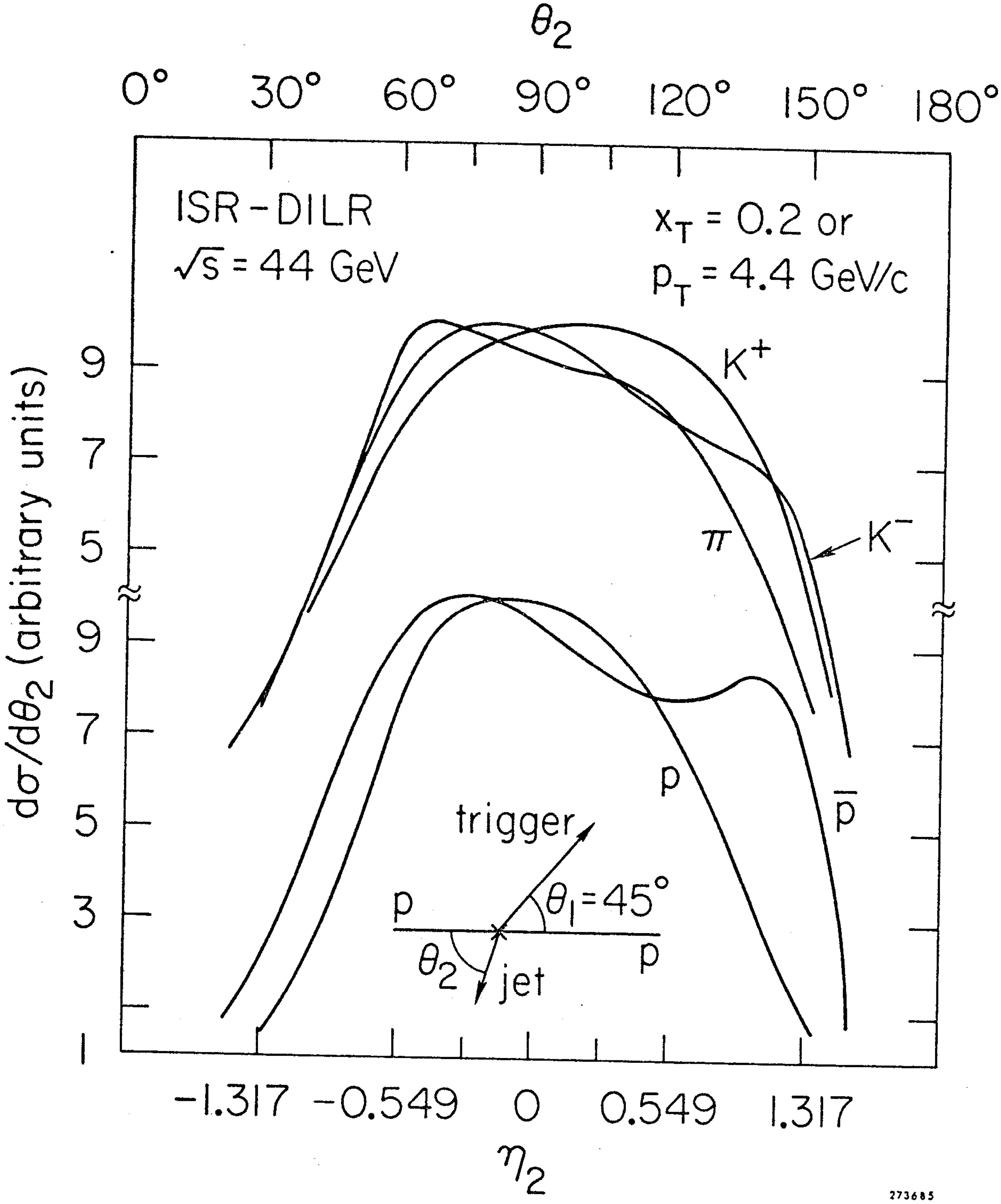

θ_2
0°
30°
60°
90°
120°
150°
180°
ISR-DILR
$\sqrt{s} = 44$ GeV
$x_T = 0.2$ or
$p_T = 4.4$ GeV/c
K^+
π
K^-
p
$\bar{p}$
trigger
$\theta_1 = 45°$
p
p
θ_2
jet
9
7
5
9
7
5
3
1
$d\sigma/d\theta_2$ (arbitrary units)
-1.317
-0.549
0
0.549
1.317
η_2

273685

Fig. 8